Electrochemistry Communications 149 (2023) 107473

Contents lists available at ScienceDirect

Electrochemistry Communications

journal homepage: www.elsevier.com/locate/elecom

Short Communication

Nanoporous boron-doped diamond produced by a combination of high-energy ion irradiation and anodization

Chenghao Lin [a], Yuki Maeda [a,1], Kuniaki Murase [a], Kazuhiro Fukami [a,b,*]

[a] Department of Materials Science and Engineering, Kyoto University, Kyoto 606-8501, Japan
[b] Integrated Research Center for Carbon Negative Science, Institute of Advanced Energy, Kyoto University, Kyoto 611-0011, Japan

ARTICLE INFO

Keywords:
Boron-doped diamond
Ion irradiation
Anodization
Nanoporous

ABSTRACT

A wide electrochemical window makes boron-doped diamond (BDD) a promising electrode material. To utilize its excellent properties, nanopore formation on the surface to increase the specific surface area is highly desirable. Although anodization has the potential to produce nanoporous structures on the surface of materials, BDD has yet to be anodized due to its high physical and chemical stability. Here, we report that high-energy Si(II) ion irradiation forms sp^2 defects, which enable the anodization of BDD, and demonstrate that this anodization results in the formation of nanoporous BDD.

1. Introduction

Diamond, which is one of the hardest substances utilized in materials processing, has potential as a next-generation, wide-gap semiconductor in energy-saving devices [1]. Boron-doped diamond (BDD) is often used as an electrode material due to its large apparent potential window owing to its low electrocatalytic activity [2]. Although BDD electrodes are strong candidates for electrochemical sensors [3–5], porosification of electrode surfaces on the nano- and micrometer scales is desired, since a large specific surface area is often an important requirement in sensor materials.

Anodization is a powerful technology used to produce nanopores on metal and semiconductor surfaces [6,7]. Although many studies have investigated anodization to form and utilize porous silicon [8–15], few have reported anodization of semiconductors with wide band gaps, mainly due to their physical and chemical stability. In spite of this stability, we previously reported that high-energy ion or mid-infrared free-electron laser irradiation can control the lattice defects and anodize silicon carbide, a well-known wide-band gap semiconductor [16,17]. Because diamond has a similar crystal structure to silicon carbide, as well as similar physical and chemical stability, a strategy utilizing high-energy ion irradiation could be applicable to the anodization of diamond.

Here, we report that a combination of high-energy Si(II) ion irradiation and anodization can produce nanoporous BDD. The formation of lattice defects in diamond, namely sp^2 carbon, promotes anodization. In contrast, anodization without high-energy ion irradiation generates a roughened and oxidized BDD surface, which is not suitable for practical electrodes. Our results clearly indicate that high-energy ion irradiation is critical to the formation of nanoporous BDD without surface oxidation.

2. Experimental

Polycrystalline BDD (NeoCoat Electrode) thin films (~2.5 μm thick) on Si(100) were used. The doping level of the BDD electrode was 2500 ppm. The working electrode was a 10 mm × 10 mm BDD substrate. The substrate was cleaned in acetone for 10 min under sonication and subsequently cleaned in a mixture of NH_4OH, H_2O_2, and H_2O with a 1:1:5 vol ratio for 5 min at 80 °C. Then the substrate was immersed in a mixture of HCl, H_2O_2, and H_2O with a 1:1:6 vol ratio for 5 min at 80 °C. All the chemicals were of analytical grade. Prior to use, the substrate was cleaned in ultrapure water for 10 min under sonication and etched for 5 min in 5 wt% HF.

High-energy Si(II) ions at 5.1 MeV (Dual-beam facility for energy science and technology; DuET, Kyoto University) were used for irradiation before anodization. Ion irradiation was conducted for 60 min at 400 °C in a vacuum with an ion flux of 8.7×10^{15} m^{-2} s^{-1}. Electrochemical measurements were carried out using a potentio-galvanostat (BioLogic Science inc. SP-150) with a three-electrode cell using Ag|

* Corresponding author at: Department of Materials Science and Engineering, Kyoto University, Kyoto 606-8501, Japan.
E-mail address: fukami.kazuhiro.2u@kyoto-u.ac.jp (K. Fukami).
[1] Present address. Central Research Institute of Electric Power Industry, Kanagawa 240-0196, Japan.

https://doi.org/10.1016/j.elecom.2023.107473
Received 8 March 2023; Accepted 21 March 2023
Available online 24 March 2023

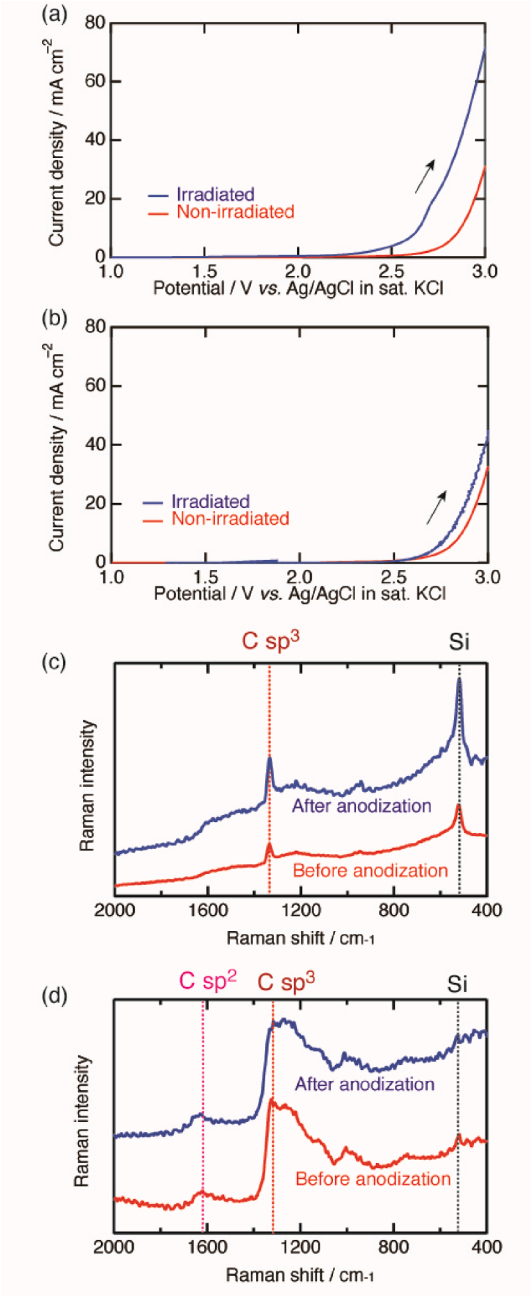

Fig. 1. Anodic linear sweep voltammograms for an electrolytic solution containing (a) acetic acid (3.0 M CH_3COOH + 1.0 M H_2SO_4) and (b) formic acid (2.0 M HCOOH + 1.0 M H_2SO_4) with and without high-energy ion irradiation. Raman spectra of BDD before and after anodization (c) without and (d) with high-energy ion irradiation.

AgCl sat. KCl and a platinum rod as the reference and counter electrodes, respectively. Note that herein all the potential values are referred to the reference electrode. The area of the working electrode was fixed at 0.196 cm^2 (5 mm ϕ). The current density values were calculated using the projected electrode area (0.196 cm^2). Anodization was performed in an electrolytic solution of 3.0 M CH_3COOH + 1.0 M H_2SO_4 at a constant current density of 0.2 A cm^{-2} for 4 h. To verify the effect of acetic acid, a different electrolytic solution of 2.0 M HCOOH + 1.0 M H_2SO_4 was tested for comparison. Linear sweep voltammograms were obtained at a scanning rate of 10 mV s^{-1}. Samples after anodization were characterized by field-emission scanning electron microscopy (FE-SEM; JEOL JSM-6500F) and scanning transmission electron microscopy (STEM; JEOL JEM-2010F), together with electron diffraction analyses, X-ray photoelectron spectroscopy (XPS; JEOL JPS-9010TRX, Al-Kα), and Raman spectroscopy (AIRIX corp., STR-CRPS-633BN-KU).

3. Results and discussion

The effect of high-energy ion irradiation on anodization behavior was investigated. Fig. 1(a) depicts the anodic linear sweep voltammograms (LSVs) using BDD electrodes with and without high-energy ion irradiation. The oxidation current begins to flow at 2.5 V without irradiation and at 2.2 V with irradiation. The difference in current density reaches 40 mA cm^{-2} at 3.0 V, demonstrating that high-energy ion irradiation promotes the anodic oxidation of BDD in a mixed solution of acetic acid and sulfuric acid. To investigate whether acetic acid enhances the electrochemical reactivity, LSVs were also measured in a mixed solution of formic acid and sulfuric acid (Fig. 1b). Compared with the results obtained using acetic acid, the promotion of anodic oxidation by high-energy ion irradiation is less pronounced, indicating that the type of carboxylic acid influences the enhancement of anodic oxidation in BDD electrodes.

To investigate the origin of the enhanced anodic oxidation, BDD electrodes were characterized by Raman spectroscopy. Fig. 1(c) shows Raman spectra of BDD without high-energy ion irradiation before and after anodization. The bands at ~520 cm^{-1} and ~1330 cm^{-1} are assigned to the phonon modes of the silicon substrate and the sp^3 hybridized carbon, respectively. No other peaks are assigned to sp^2 and sp hybridization.

Fig. 1(d) depicts the corresponding spectra with high-energy ion irradiation. The sp^3 band is apparent, but the peak width increases significantly compared to the spectra without high-energy ion irradiation. The broadening of the sp^3 peak is attributed to lattice defects induced by ion irradiation [18]. Because the peak at ~1620 cm^{-1} is often observed in graphite (sp^2 hybridized carbon) with structural defects [19], the lattice defects are formed by ion irradiation. Since the Raman band at ~1620 cm^{-1} remains after anodization, high-energy ion irradiation produces defects in the interior of the BDD film with localized graphitization and not on the outermost surface.

Fig. 2 shows typical surface morphologies of BDD electrodes anodized in an electrolytic solution containing acetic acid. These images were acquired by FE-SEM and cross-sectional STEM. Comparing Fig. 2(a) and 2(b) shows that the BDD surface dissolves electrochemically even without high-energy ion irradiation. Fig. 2(b) strongly suggests that the dissolution rate depends upon the crystal faces exposed to the solution. In contrast, anodization has a negligible effect on the macroscopic surface morphologies of irradiated BDD (Fig. 2c and 2d); however, the crystal grains after anodization formed numerous nanopores, even though the pore size is too small to be observed by FE-SEM. Anodization randomly roughens the BDD surface, even without high-energy ion irradiation (Fig. 2e and 2f). Thus, anodization of BDD without ion irradiation increases the surface roughness due to crystal-face-dependent dissolution. Anodizing the high-energy ion irradiated BDD electrode forms a surface containing many nanopores with a relatively constant diameter of 10 nm (Fig. 2h). Hence, high-energy ion irradiation suppresses the crystal-plane-dependent dissolution while promoting self-organized dissolution to form nanopores.

To understand the properties of BDD electrodes, Fig. 3(a) and 3(b) show XPS C1s and C2p spectra before and after high-energy ion irradiation. As a result of high-energy ion irradiation, the peaks shift ~1.1 eV to higher binding energies, suggesting that the Fermi level increases and the BDD electrode should behave more like an intrinsic semiconductor. However, the modified Fermi level itself cannot explain the enhanced anodic oxidation of BDD. Fig. 3(c) shows the XPS C1s spectrum of a BDD electrode without high-energy ion irradiation and its deconvolution. The peak comprises the contributions of sp^3 carbon in the bulk and the C—H_x bond on the surface of BDD. Anodizing without high-energy ion irradiation induces a new peak as a shoulder as shown in Fig. 3(d). Using

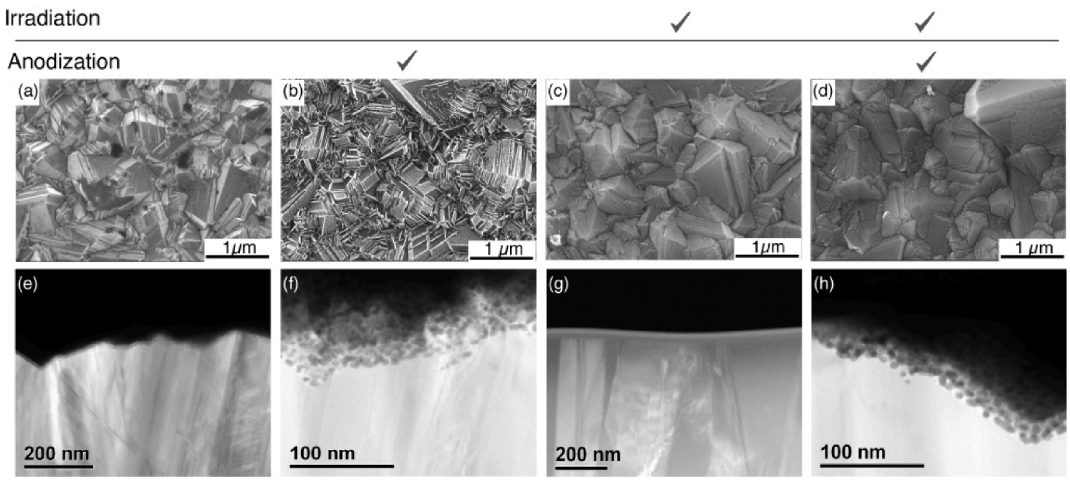

Fig. 2. FE-SEM images of the top surface of BDD acquired before anodization (a) without and (c) with high-energy ion irradiation, and after anodization (b) without and (d) with high-energy ion irradiation. Cross-sectional STEM images acquired before anodization (e) without and (g) with high-energy ion irradiation, and after anodization (f) without and (h) with high-energy ion irradiation.

an electron flood gun for neutralization during the XPS measurement shifts the main peak at 286 eV to a slightly lower binding energy but the shoulder is unaffected (Fig. 3d), indicating that differential charging on the surface of BDD occurs after anodization without high-energy ion irradiation. Under such differential charging, the spectrum cannot be deconvoluted. Fig. 3(e) is a typical C1s spectrum obtained after high-energy ion irradiation without anodization. Deconvolution reveals a non-negligible contribution of sp^2 carbon. The results shown in Figs. 1 (d) and 3(e) suggest that the sp^2 carbon contribution comes from defects formed by high-energy ion irradiation.

Fig. 3(f) shows the C1s spectrum after anodization of the irradiated BDD. The C—H_x bond is the main contributor to the peak followed by the sp^3 carbon and then some oxidated species. Since the C—H_x bond exists on the surface of BDD, the drastic increase in the contribution of C—H_x means that the surface area of BDD increases due to the combination of high-energy ion irradiation and anodization. Fig. 4(a) shows the electron diffraction pattern of a sample near the top surface without high-energy ion irradiation after anodization. The diffraction is weak and unclear, suggesting that crystalline and amorphous regions coexist in the analyzed area. In contrast, the diffraction remains clear after anodizing using a BDD with high-energy ion irradiation (see Fig. 4b).

Based on these results, a mechanism explaining the enhancement of anodic oxidation of BDD by high-energy ion irradiation is proposed. In previous studies on BDD corrosion, Kashiwada and coworkers found that corrosion occurs in a solution containing acetic acid, but not in a solution with formic acid [20]. They concluded that BDD corrosion is triggered by methyl radicals electrochemically formed by Kolbe electrolysis. Methyl radicals attack the BDD surface, forming dangling bonds. The dangling bonds are then stabilized by forming sp^2 carbon. Thus, the corrosion reaction occurs stepwise on the surface of the BDD. By contrast, in our experiments, sp^2 carbon is pre-formed inside the BDD by high-energy ion irradiation prior to anodization. Consequently, exposing the sp^2 carbon in the bulk BDD to the electrolytic solution greatly enhances the anodic oxidation of BDD. It is likely that the anodic reaction causes the frontier to intrude into the BDD bulk. Unfortunately, we have yet to produce much deeper nanoporous BDD since prolonged anodization causes the nanopores to disappear, which is probably due to electropolishing of BDD.

Although high-energy ion irradiation forms defects in BDD, the defect density is not uniform along the thickness of BDD. The number of defects increases as the distance from the surface to the BDD bulk increases [21]. It is likely that a threshold defect density to achieve nanopore formation exists. Above the threshold density, the anodization reaction occurs uniformly on the surface, which leads to the disappearance of the nanopores.

4. Conclusion

Nanoporous diamond is formed by anodization for the first time. The key to anodization is the localized formation of sp^2 carbons upon high-energy ion irradiation, which act as the reaction centers. Although anodization occurs under limited conditions, the results in this study should trigger more research on nanoporous diamond formation by anodization and may eventually enable control of the pore diameter and depth.

CRediT authorship contribution statement

Chenghao Lin: Investigation, Validation, Writing – original draft. **Yuki Maeda:** Validation, Writing – review & editing. **Kuniaki Murase:** Validation, Writing – review & editing. **Kazuhiro Fukami:** Conceptualization, Methodology, Writing – original draft, Supervision, Project administration, Funding acquisition.

Declaration of Competing Interest

The authors declare that they have no known competing financial interests or personal relationships that could have appeared to influence the work reported in this paper.

Data availability

Data will be made available on request.

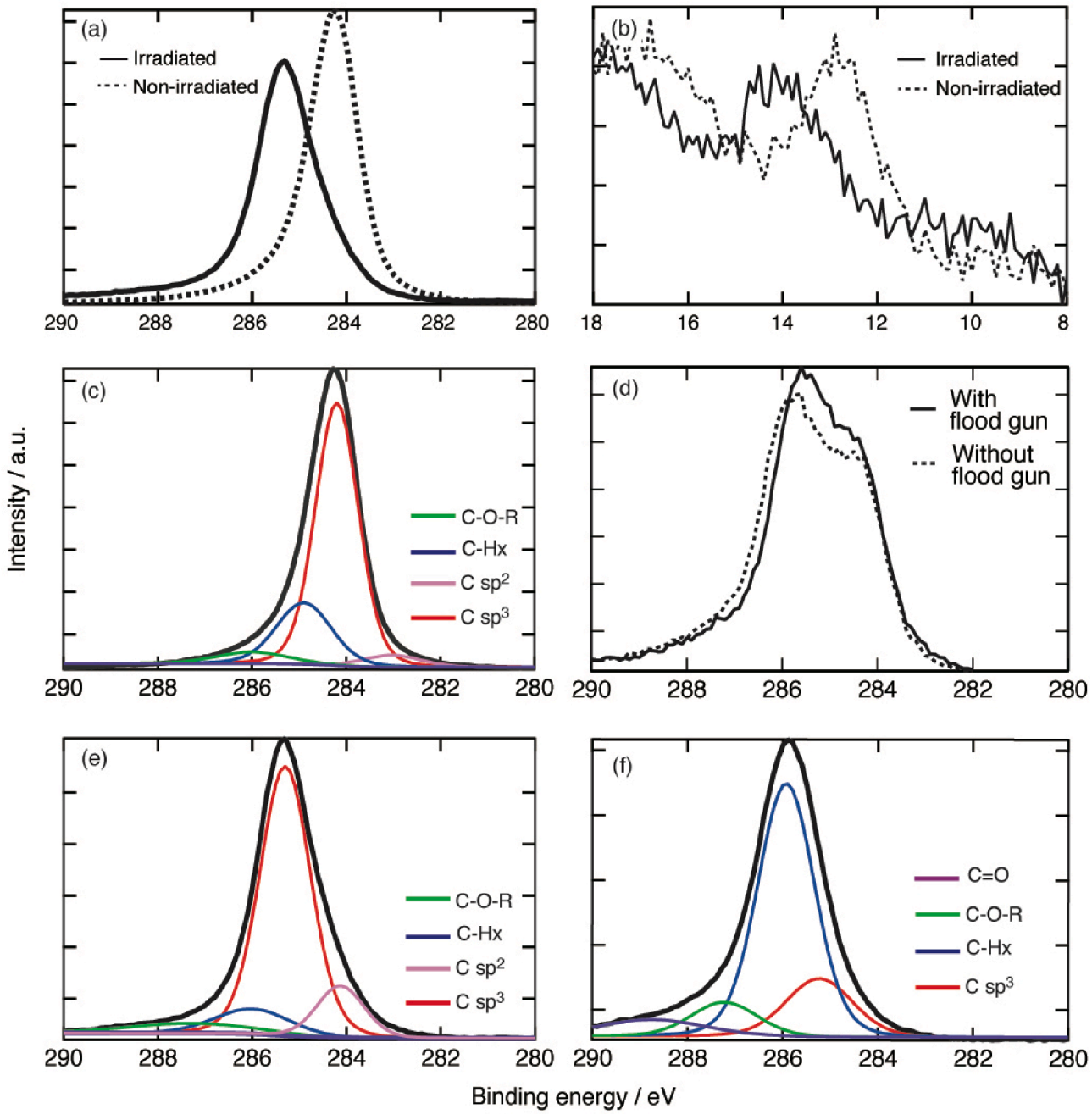

Fig. 3. XPS spectra of BDD. Spectra (a) C1s and (b) C2p, respectively, with and without high-energy ion irradiation. (c) C1s spectrum with the deconvolution of the as-prepared BDD without high-energy ion irradiation and anodization. (d) Spectrum of BDD without high-energy ion irradiation after anodization. (e) C1s spectrum with the deconvolution of BDD with high-energy ion irradiation but without anodization. (f) C1s spectrum with the deconvolution of BDD with high-energy ion irradiation after anodization.

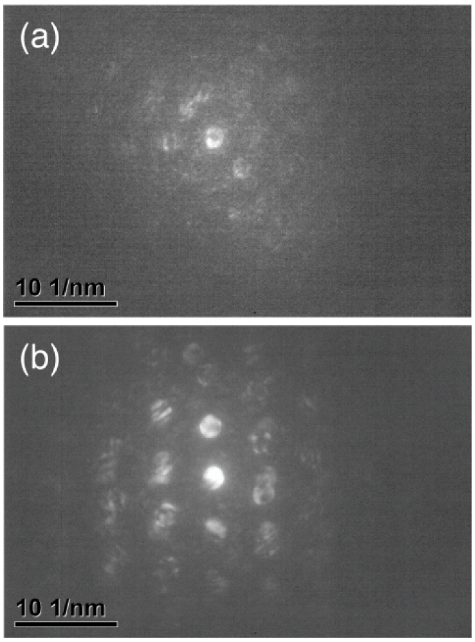

Fig. 4. Nanobeam diffraction of anodized BDD electrodes. Diffraction near the top surface of BDD (a) without and (b) with high-energy ion irradiation.

Acknowledgment

This work was supported by a JSPS Grant-in-Aid for Scientific Research B (Grant Number 21H01670; K.F.) and the Joint Usage/Research Program on Zero-Emission Energy Research, Institute of Advanced Energy, Kyoto University.

References

[1] S. Fujita, Wide-bandgap semiconductor materials: for their full bloom, Jpn. J. Appl. Phys. 54 (3) (2015) 030101.
[2] H.B. Martin, A. Argoitia, U. Landau, A.B. Anderson, J.C. Angus, Hydrogen and oxygen evolution on boron-doped diamond electrodes, J. Electrochem. Soc. 143 (6) (1996) L133–L136.
[3] Y. Einaga, Diamond electrodes for electrochemical analysis, J. Appl. Electrochem. 40 (2010) 1807–1816, https://doi.org/10.1007/s10800-010-0112-z.
[4] P.F. Pereira, W.P. Da Silva, R.A.A. Muñoz, E.M. Richter, A simple and fast batch injection analysis method for simultaneous determination of phenazopyridine, sulfamethoxazole, and trimethoprim on boron-doped diamond electrode, J. Electroanal. Chem. 766 (2016) 87–93, https://doi.org/10.1016/j.jelechem.2016.01.034.
[5] R.F. Brocenschi, T.A. Silva, B.C. Lourencao, O. Fatibello-Filho, R.C. Rocha-Filho, Use of a boron-doped diamond electrode to assess the electrochemical response of the naphthol isomers and to attain their truly simultaneous electroanalytical determination, Electrochim. Acta 243 (2017) 374–381, https://doi.org/10.1016/j.electacta.2017.05.044.
[6] H. Föll, S. Langa, J. Carstensen, M. Christophersen, I.M. Tiginyanu, Pores in III-V semiconductors, Adv. Mater. 15 (2003) 183–198.
[7] G. Flamand, J. Poortmans, K. Dessein, Formation of porous Ge using HF-based electrolytes, Phys. Status Solidi C 2 (2005) 3243–3247, https://doi.org/10.1002/pssc.200461130.
[8] H. Föll, M. Christophersen, J. Carstensen, G. Hasse, Formation and application of porous silicon, Mater. Sci. Eng. R Rep. 39 (2002) 93–141, https://doi.org/10.1016/s0927-796x(02)00090-6.
[9] K. Fukami, F.A. Harraz, T. Yamauchi, T. Sakka, Y.H. Ogata, Fine-tuning in size and surface morphology of rod-shaped polypyrrole using porous silicon as template, Electrochem. Commun. 10 (2008) 56–60, https://doi.org/10.1016/j.elecom.2007.10.019.
[10] K. Fukami, K. Kobayashi, T. Matsumoto, Y.L. Kawamura, T. Sakka, Y.H. Ogata, Electrodeposition of noble metals into ordered macropores in p-type silicon, J. Electrochem. Soc. 155 (2008) D443–D448, https://doi.org/10.1149/1.2898714.
[11] K. Fukami, Y. Tanaka, M.L. Chourou, T. Sakka, Y.H. Ogata, Filling of mesoporous silicon with copper by electrodeposition from an aqueous solution, Electrochim. Acta 54 (2009) 2197–2202, https://doi.org/10.1016/j.electacta.2008.10.024.
[12] A. Koyama, K. Fukami, Y. Suzuki, A. Kitada, T. Sakka, T. Abe, K. Murase, M. Kinoshita, High-rate charging of zinc anodes achieved by tuning hydration properties of zinc complexes in water confined within nanopores, J. Phys. Chem. C 120 (2016) 24112–24120, https://doi.org/10.1021/acs.jpcc.6b07030.
[13] T. Yasuda, Y. Maeda, K. Matsuzaki, Y. Okazaki, R. Oda, A. Kitada, K. Murase, K. Fukami, Spontaneous symmetry breaking of nanoscale spatiotemporal pattern as the origin of helical nanopore etching in silicon, ACS Appl. Mater. Interfaces 11 (2019) 48604–48611, https://doi.org/10.1021/acsami.9b18025.
[14] Y. Maeda, T. Yasuda, K. Matsuzaki, Y. Okazaki, E. Pouget, R. Oda, A. Kitada, K. Murase, G. Raffy, D.M. Bassani, K. Fukami, Common mechanism for helical nanotube formation by anodic polymerization and by cathodic deposition using helical pores on silicon electrodes, Electrochem. Commun. 114 (2020), 106714, https://doi.org/10.1016/j.elecom.2020.106714.
[15] M.P. Stewart, J.M. Buriak, Chemical and biological applications of porous silicon technology, Adv. Mater. 12 (2000) 859–869, https://doi.org/10.1002/1521-4095(200006)12:12<859::AID-ADMA859>3.0.CO;2-0.
[16] Y. Maeda, Á. Munõz-Noval, E. Suzuki, S. Kondo, A. Kitada, S. Shiki, M. Ohkubo, S. Hayakawa, K. Murase, K. Fukami, Macroporous SiC formation in anodizing triggered by irradiation-induced lattice defects, J. Phys. Chem. C 124 (2020) 11032–11039, https://doi.org/10.1021/acs.jpcc.0c02491.
[17] Y. Maeda, H. Zen, A. Kitada, K. Murase, K. Fukami, Enhancement of oxidation of silicon carbide originating from stacking faults formed by mode-selective phonon excitation using a mid-infrared free electron laser, J. Phys. Chem. Lett. 13 (2022) 2956–2962, https://doi.org/10.1021/acs.jpclett.2c00464.
[18] N.M. Kazuchits, O.V. Korolik, M.S. Rusetsky, V.N. Kazuchits, N.S. Kirilkin, V. A. Skuratov, Raman scattering in diamond irradiated with high-energy xenon ions, Nucl. Instruments Methods Phys. Res. Sect. B Beam Interact. Mater. Atoms 472 (2020) 19–23, https://doi.org/10.1016/j.nimb.2020.03.034.
[19] M. Chen, J.P. Best, I. Shorubalko, J. Michler, R. Spolenak, J.M. Wheeler, Influence of helium ion irradiation on the structure and strength of diamond, Carbon 158 (2020) 337–345, https://doi.org/10.1016/j.carbon.2019.10.078.
[20] T. Kashiwada, T. Watanabe, Y. Ootani, Y. Tateyama, Y. Einaga, A study on electrolytic corrosion of boron-doped diamond electrodes when decomposing organic compounds, ACS Appl. Mater. Interfaces 8 (2016) 28299–28305, https://doi.org/10.1021/acsami.5b11638.
[21] D.P. Hickey, K.S. Jones, R.G. Elliman, Amorphization and graphitization of single-crystal diamond - a transmission electron microscopy study, Diam. Relat. Mater. 18 (2009) 1353–1359, https://doi.org/10.1016/j.diamond.2009.08.012.